Distributed Control of Coupled Inhomogeneous Diffusion in Tokamak Plasmas

Bojan Mavkov, Emmanuel Witrant, and Christophe Prieur

Abstract— This article proposes novel distributed control methods for the coupled dynamics of the safety factor and electron temperature profiles in tokamaks. The feedback design is based on an infinite-dimensional setting using the Lyapunov analysis for partial differential equations. The coupled dynamics is modeled by two 1-D linearized resistive diffusion equations. We first propose a combined control of both dynamics based on stability analysis. A composite control is then synthesized using a singular perturbation theory where the fast component of the electron temperature is decoupled from the slow component induced by the magnetic field dynamics. Both control methods are evaluated using the RApid Plasma Transport simulatOR simulator and applied to the International Thermonuclear Experimental Reactor tokamak device. The distributed control is performed using antennas operated at electron cyclotron frequency.

Index Terms— Controlled thermonuclear fusion, distributed control methods, partial differential equations (PDEs), singular perturbation theory, tokamak devices.

I. INTRODUCTION

TOKAMAKS are large devices using a magnetic field to confine a hot plasma in the shape of a torus. Tokamak research aims at building a reliable power production system using controlled thermonuclear fusion [30]. Heating of the plasma comes from the electric currents obtained from several sources. The main source of current in a tokamak is the one induced by the transformer action caused by the central ohmic coil. Other sources of current are neutral-beam injection and radio frequency (RF) antennas. There are several plasma parameters, such as the safety factor q (related to the magnetic flux) and the temperature of the electrons T_e that are defining the plasma state. Achieving a long term steady-state fusion reaction relies on advanced tokamak operation scenarios in which the profiles of q and T_e are optimized.

Simultaneous control of multiple plasma parameters profiles is a challenge, in particular because of the coupling between the magnetic flux and the pressure profiles. The safety factor is crucial to analyze magnetohydrodynamics stability and performance. The plasma resistivity, which governs the evolution of q [26], depends primarily on T_e. The dynamics of q and T_e are thus highly coupled. In this article, we focus on the simultaneous control of the poloidal magnetic flux gradient z and the electron temperature T_e. These two parameters

are modeled by nonlinear coupled resistive diffusion partial differential equations (PDEs).

Numerous results were obtained on designing control algorithms for the safety factor profile using multi-input multi-output (MIMO) lumped models [2], [3], [20], [22], [29]. A simple control algorithm based on the singular value decomposition of the experimentally deduced linear static response model for integrated control of q and T_e profiles is given in [18]. A control algorithm for simultaneous control of the q and T_e profiles, based on an MIMO approach for finite-dimensional systems with a first principles model, is presented in [1].

In this article, we focus on developing control algorithms based on the infinite-dimensional control theory. Several works used this method to control the safety factor profile [4], [11], [13], with different levels of simplification regarding the impact of the temperature profile (through the plasma resistivity and the bootstrap currents). Nevertheless, this article is the first, to the best of our knowledge, to consider the stability and control of the coupled dynamics in the PDE framework. We consider diffusion coefficients that vary in space and time and extend the infinite-dimensional Lyapunov analysis proposed in [4] to the system given by the two coupled PDEs for z and T_e profiles. We examine the stability of the nominal system and design a control strategy that improves the convergence rate to the desired equilibrium point.

Two control strategies are proposed: one based on a single control Lyapunov function for both variables and one that decouples the variables using the singular perturbation theory. The first method is suitable for small tokamaks, while the second is more suitable for large tokamaks, for which the difference between the time scales of the two states is larger. Singular perturbation theory is widely used in a control system theory [12], [17], [19]. Research works in boundary control of singularly perturbed PDEs with constant transport coefficients are introduced in [27] and [28]. We propose a composite control strategy, where separate controls are calculated for the slow and fast dynamics of the system while taking into account the space variations of the coefficients.

The control methods developed, in this article, are implemented on RApid Plasma Transport simulatOR (RAP-TOR) [9], a control-oriented, physics-based 1-D code modeling the coupled q and T_e transport. The transport equations used in this simulator are nonlinear and tuned to match the data coming from real operating tokamaks [14]. The code is used as a tool for designing real-time control applications, fast plasma simulation and as a real-time estimator running in parallel with the plasma discharge in TCV tokamak. Our control results are evaluated on the International

Thermonuclear Experimental Reactor (ITER) simulations using RAPTOR. ITER is the leading research tokamak that aims to prove the feasibility of using thermonuclear fusion for energy production.

This article is organized as follows. In Section II, the coupled PDEs for z and T_e are presented and the control problem is defined. In Section III, the simplified linearized model is derived. A Lyapunov function for stability analysis is computed for the linearized dynamics and used for convergence rate control in Section IV. In Section V, the model is decoupled using the singular perturbation theory and composite control is computed for the decoupled linearized system. The control implementation is presented in Section VI. In Section VII, the results from the control implemented in the nonlinear RAPTOR simulator are presented. Due to space limitation, some proofs and results are omitted. See [24] for a full version of this article.

II. PROBLEM DESCRIPTION

A. Magnetic Flux Dynamics

For control design, we are interested in the evolution of the safety factor $q = (\partial \Phi/\partial \Psi) = (2\pi B_0 \, a^2 \, x/(\partial \Psi/\partial x))$ (or its reciprocal, the rotational transform ι), which is one of the key parameters to analyze the plasma stability and transport. The safety factor q denotes the ratio of toroidal to poloidal turns for a given magnetic field surface within a tokamak. Ψ is the poloidal magnetic flux, Φ is toroidal magnetic flux, B_0 is the toroidal magnetic field at the center of the vacuum vessel, and $x = \rho/a$ is a normalized variable of the equivalent radius of the magnetic surfaces, $\rho = (\Phi/\pi B_0)^{1/2}$ and a being the small plasma radius.

We control q through the space derivative of the magnetic flux $z = (\partial \Psi/\partial x)$. To design a control law with real-time capabilities, we consider the simplified 1-D model for z (using the cylindrical approximation, which can be easily alleviated but simplifies the notations) as in [31]

$$\frac{\partial z}{\partial t} = \frac{\partial}{\partial x}\left(\frac{\eta_{\|}}{\mu_0 a^2 x}\frac{\partial}{\partial x}(xz)\right) + \frac{\partial}{\partial x}(\eta_{\|} R_o j_{\mathrm{ni}}) \qquad (1)$$

with boundary conditions $z(0, t) = 0$ and $z(1, t) = -(R_o \mu_0 \, I_p(t)/2\pi)$, $\forall t \geq 0$, and initial condition $z(x, 0) = z_0(x)$, $\forall x \in [0, 1]$. R_0 is the major radius of the plasma (assumed constant in time), μ_0 is the permeability of vacuum, and $\eta_{\|}(x, t)$ is the parallel electrical resistivity of the plasma. $I_p(t)$ is the total plasma current and $j_{\mathrm{ni}}(x, t)$ is the noninductive current density. The noninductive current density is obtained by combining the auxiliary sources of current density $j_{\mathrm{aux}}(x, t)$ (current drive RF systems) and the bootstrap current density $j_{\mathrm{bs}}(x, t)$ as $j_{\mathrm{ni}} = j_{\mathrm{aux}} + j_{\mathrm{bs}}$. The parameters $\eta_{\|}(x, t)$ and $j_{\mathrm{bs}}(x, t)$ are highly dependent on the dynamics of the electron temperature $T_e(x, t)$. Simplified models for these parameters are given in [24].

B. Electron Temperature Dynamics

The transport phenomena of the electrons temperature T_e and density n_e are coupled and modeled by a diffusion equation. This equation is obtained from simplified 1-D energy transport and is presented as in [15], using the cylindrical approximation, as

$$\frac{3}{2}\frac{\partial (n_e T_e)}{\partial t} = \frac{1}{a^2}\frac{1}{x}\frac{\partial}{\partial x}\left(x n_e \chi_e \frac{\partial T_e}{\partial x}\right) + Q_e \qquad (2)$$

with boundary conditions $(\partial T_e/\partial x)(0, t) = 0$ and $T_e(1, t) = T_{e,\mathrm{edge}}(t)$, $\forall t \geq 0$, and initial condition $T_e(x, 0) = T_0(x)$, $\forall x \in [0, 1]$. $\chi_e(x, t)$ is the electron diffusivity and $Q_e(x, t)$ is the total electron heating power density. Note that χ_e and Q_e depend on both z and T_e, rendering the system coupled and nonlinear. The net electron heating energy source Q_e results from several power densities: $Q_e = Q_{\mathrm{OH}} - Q_{ei} - Q_{\mathrm{rad}} + Q_{\mathrm{aux}}$, where $Q_{\mathrm{OH}}(x, t)$ is the ohmic effect, $Q_{ei}(x, t)$ is the electron-ion heat exchange, $Q_{\mathrm{rad}}(x, t)$ is the radiation (their simplified models are given in [24]), and $Q_{\mathrm{aux}}(x, t)$ comes from the auxiliary sources.

Auxiliary actuators (such as neutral beam injection and RF antennas operated at ion cyclotron, electron cyclotron (EC), or lower hybrid frequencies) may act both on the current density $j_{\mathrm{aux}}(x, t)$ and on the power density $Q_{\mathrm{aux}}(x, t)$, with a relative effect that depends on the nature of the actuator. The distributed controlled inputs $j_{\mathrm{aux}}(x, t)$ and $Q_{\mathrm{aux}}(x, t)$ thus depend on the same limited set of engineering variables $u(t)$, optimized to set the desired auxiliary profiles.

The goal of this article is to design a control strategy for the coupled dynamics of the inverse of the safety factor ι (proportional to z) and the electron temperature T_e using $u(t)$.

III. LINEARIZED COUPLED DYNAMICS

For control purpose, we linearize the model at a given equilibrium state $(\bar{z}, \bar{T}_e)$ corresponding to the constant inputs $\bar{u}$ and $\bar{I}_p$. An equilibrium is defined as a stationary solution of (1) and (2) as

$$\begin{cases} 0 = \dfrac{\partial}{\partial x}\left(\dfrac{\bar{\eta}_{\|}}{\mu_0 a^2 x}\dfrac{\partial}{\partial x}(x\bar{z})\right) + \dfrac{\partial}{\partial x}(\bar{\eta}_{\|} R_o \bar{j}_{\mathrm{ni}}) \\ 0 = \dfrac{1}{a^2}\dfrac{1}{x}\dfrac{\partial}{\partial x}\left(x n_e \bar{\chi}_e \dfrac{\partial \bar{T}_e}{\partial x}\right) + \bar{Q}_e. \end{cases} \qquad (3)$$

The linearized model is derived around $(\bar{z}, \bar{T}_e)$ by substituting, in the reference model from Section II, $z = \bar{z} + \tilde{z}$, $T_e = \bar{T}_e + \tilde{T}_e$, $u = \bar{u} + \tilde{u}$, and $I_p = \bar{I}_p + \tilde{I}_p$, and using Taylor series with first order approximation. $(\tilde{z}, \tilde{T}_e, \tilde{u}, \tilde{I}_p)$ thus denotes the variations around the equilibrium. The model is further simplified by considering the following assumptions.

1) The electron density profile is constant during the heat process, $n_e = n_e(x)$.
2) The space variations of the electron density are neglected with respect to those of the temperature: $\partial n_e/\partial x \ll \partial T_e/\partial x$.
3) Only the auxiliary heating/current drive systems are considered as controlled inputs, while I_p is assigned with a reference value, $I_p(t) = \bar{I}_p$. Note that $I_p(t)$ could be used as a controlled input in our framework using the methods described in [7].

This article has been accepted for inclusion in a future issue of this journal. Content is final as presented, with the exception of pagination.

MAVKOV *et al.*: DISTRIBUTED CONTROL OF COUPLED INHOMOGENEOUS DIFFUSION IN TOKAMAK PLASMAS 3

Under these assumptions, the simplified linearized coupled model coming from (1) and (2) is derived as

$$
\begin{cases}
\dfrac{\partial \tilde{z}}{\partial t} = \dfrac{\partial}{\partial x}\left(\dfrac{a_1(x)}{x}\dfrac{\partial}{\partial x}(x\tilde{z})\right) + \dfrac{\partial}{\partial x}\left(a_2(x)\tilde{T}_e\right) \\
\qquad + \dfrac{\partial}{\partial x}\left(a_3(x)\dfrac{\partial \tilde{T}_e}{\partial x}\right) + \dfrac{\partial}{\partial x}\left(a_4(x)\tilde{z}\right) \\
\qquad + \dfrac{\partial}{\partial x}\left(a_5(x)\tilde{j}_{\text{aux}}(u,x,t)\right) \\
\varepsilon\dfrac{\partial \tilde{T}_e}{\partial t} = \dfrac{1}{x}\dfrac{\partial}{\partial x}\left(xb_1(x)\dfrac{\partial \tilde{T}_e}{\partial x}\right) - b_2(x)\tilde{T}_e \\
\qquad + \dfrac{1}{x}\dfrac{\partial}{\partial x}\left(xb_3(x)\tilde{z}\right) + \dfrac{b_4(x)}{x}\left(\dfrac{\partial}{\partial x}(x\tilde{z})\right) \\
\qquad + b_5(x)\tilde{Q}_{\text{aux}}(u,x,t)
\end{cases}
\tag{4}
$$

with boundary conditions, $\forall t \geq 0$

$$
\tilde{z}(0,t) = \tilde{z}(1,t) = \dfrac{\partial \tilde{T}_e}{\partial x}(0,t) = 0,\ \tilde{T}_e(1,t) = \tilde{T}_{e,\text{edge}}(t) \tag{5}
$$

and initial conditions

$$
\tilde{z}(x,t_0) = \tilde{z}_0;\ \tilde{T}_e(x,t_0) = \tilde{T}_{e,0}\ \ \forall x \in [0,1]. \tag{6}
$$

The coefficients of these PDEs $a_i(x)$ and $b_i(x)$ are given in [24]. ε is the typical ratio between the energy confinement time and the characteristic resistive diffusion time, which varies with the size of the tokamak. In a small tokamak such as TCV $\varepsilon \approx 0.07$ while in a large tokamak such as ITER, this $\varepsilon \approx 0.01$. The relative time constants of the dynamics and the impact of the couplings between the states are thus very diverse.

IV. STABILITY ANALYSIS AND CONTROL OF THE COUPLED SYSTEM

A. Stability Analysis

The stability of the coupled dynamics is analyzed with the following Lyapunov function candidate:

$$
V(\tilde{z},\tilde{T}_e) = \dfrac{1}{2}\int_0^1 [\tilde{z}\ \ \tilde{T}_e]\begin{bmatrix} x^2\,p_1(x) & 0 \\ 0 & \gamma x^2\,p_2(x)\end{bmatrix}\begin{bmatrix}\tilde{z}\\\tilde{T}_e\end{bmatrix}dx \tag{7}
$$

where $p_1(x) > 0$ and $p_2(x) > 0$ for $x \in [0,1]$ are polynomial functions. The candidate Lyapunov function is chosen as a weighted $L^2(0,1)$ norm, and it is multiplied by the term x

to handle the singularity at $x = 0$, which comes from the cylindrical representation of the system. The scaling parameter γ is added to balance the differences of amplitude between $\tilde{z}$ and $\tilde{T}_e$. The stability of our coupled system of linearized equations is established with the following theorem.

Theorem 1: Suppose that for a given positive number α_1, there exist polynomials p_1 and p_2 such that $p_1(x) > 0$ and $p_2(x) > 0$ for all $x \in [0,1]$, and

$$
A_1(x) + \alpha_1 A_2(x) \leq 0 \tag{8}
$$

for all $x \in [0,1]$, where

$$
A_1(x) = \begin{bmatrix} A_{1,1}(x) & A_{1,2}(x) & A_{1,3}(x) & A_{1,4}(x) \\ A_{1,2}(x) & A_{2,2}(x) & A_{2,3}(x) & 0 \\ A_{1,3}(x) & A_{2,3}(x) & A_{3,3}(x) & A_{3,4}(x) \\ A_{1,4}(x) & 0 & A_{3,4}(x) & A_{4,4}(x) \end{bmatrix} \tag{9}
$$

$$
A_2(x) = \dfrac{1}{2}\begin{bmatrix} x^2 & 0 & 0 & 0 \\ 0 & \gamma x^2 & 0 & 0 \\ 0 & 0 & 0 & 0 \\ 0 & 0 & 0 & 0 \end{bmatrix} \tag{10}
$$

and the elements in the $A_1(x)$ matrix are given in (11), as shown at the bottom of this page. Then, the time derivative $\dot{V}$ of V defined in (7) along the solutions of (4) and (5) verifies

$$
\dot{V} \leq \dfrac{-\alpha_1}{\max\limits_{x\in[0,1]}\big(p_1(x),p_2(x)\big)}V
$$
$$
+ \int_0^1 x^2 p_1(x)\dfrac{\partial}{\partial x}\left(a_4(x)\tilde{j}_{\text{aux}}(\tilde{u},x,t)\right)\tilde{z}dx
$$
$$
+ \gamma\int_0^1 \dfrac{x^2 p_2(x)}{\varepsilon}b_5(x)\tilde{Q}_{\text{aux}}(\tilde{u},x,t)\tilde{T}_e dx\ \ \forall t \geq 0. \tag{12}
$$

Proof: See [24]. □

The nominal stability ($\tilde{u} = 0$) is then directly obtained with the following corollary.

Corollary 1: If the conditions of Theorem 1 are satisfied, the system (4) with $\tilde{u} = 0$, boundary conditions (5), and initial conditions (6) is globally exponentially stable. The convergence rate of the system satisfies $V(t) \leq e^{-\beta_1 t}V(\tilde{z}_0,\tilde{T}_{e,0})$, where $\beta_1 = -\alpha_1/[\max\limits_{x\in[0,1]}(p_1(x),p_2(x))]$.

Proof: This result is directly obtained by setting $\tilde{u} = 0$: the variations of the auxiliary current and power density are zero ($\tilde{j}_{\text{aux}} = \tilde{Q}_{\text{aux}} = 0$), and from Theorem 1, we obtain the

$$
A_{1,1} = \dfrac{1}{2}\big(3xp_1'(x) + x^2 p_1''(x) - p_1(x)\big)a_1(x) + \dfrac{1}{2}a_1'(x)\big(x^2 p_1'(x) + 3xp_1(x)\big) - 2xp_1(x)a_4(x) - x^2 p_1'(x)a_4(x)
$$

$$
A_{1,2} = -xp_1(x)a_2(x) - \dfrac{1}{2}x^2 p_1'(x)a_2(x) + \dfrac{\gamma}{2\varepsilon}xb_3(x)\big(xp_2'(x) + p_2(x)\big) + \dfrac{\gamma}{2\varepsilon}xp_2(x)b_4(x)
$$

$$
A_{1,3} = -\dfrac{1}{2}x^2 p_1(x)a_4(x),\quad A_{1,4} = -xp_1(x)a_3(x) - \dfrac{1}{2}x^2 p_1'(x)a_3(x)
$$

$$
A_{2,2} = -\dfrac{\gamma}{\varepsilon}x^2 p_2(x)b_2(x) + \dfrac{\gamma}{2\varepsilon}b_1(x)\big(x^2 p_2''(x) + 2xp_2'(x) + p_2(x)\big) + \dfrac{\gamma}{2\varepsilon}b_1'(x)\big(x^2 p_2'(x) + xp_2(x)\big)
$$

$$
A_{2,3} = -\dfrac{1}{2}x^2 p_1(x)a_2(x) - \dfrac{\gamma}{2\varepsilon}x^2 b_3(x)p_2(x) + \dfrac{\gamma}{2\varepsilon}x^2 p_2(x)b_4(x)
$$

$$
A_{3,3} = -x^2 p_1(x)a_1(x),\quad A_{3,4} = -\dfrac{1}{2}x^2 p_1(x)a_4(x),\quad A_{4,4} = -\dfrac{\gamma}{\varepsilon}x^2 b_1(x)p_2(x) \tag{11}
$$

inequality $\dot{V} \leq -\beta_1 V$, $\forall t \geq 0$. Integrating this inequality over time implies the desired inequality on $V(t)$. $\square$

B. Calculation of the Lyapunov Function

Using Legendre polynomials for p_1 and p_2, the inequality (8) is formulated and solved as an LMI problem defined with x in the range [0, 1]. Legendre polynomials are orthogonal in the range $[-1, 1]$, and the polynomials p_1 and p_2 can be expanded in this interval in terms of them as [16]

$$p_1(x) = \sum_{i=0}^{N_1} c_{1,i} P_i(x), \quad p_2(x) = \sum_{i=0}^{N_2} c_{2,i} P_i(x)$$

where $c_{1,1}, \ldots, c_{1,N_1}$ and $c_{2,1}, \ldots, c_{2,N_2}$ are some constant coefficients, $P_i(x)$ is the ith-order Legendre polynomial, and N_1 and N_2 are the orders of the Legendre polynomials for p_1 and p_2, respectively.

Sampling the interval [0, 1] and representing p_1 and p_2 as a sum of Legendre polynomials permit us to formulate the following LMI problem:

$$\max \alpha_1 \geq 0$$

such that the polynomials $p_1(x)$ and $p_2(x)$ satisfy, for all $x \in [0, 1]$:

1) $0 < p_1(x) \leq p_{1,\max}$ and $0 < p_2(x) \leq p_{2,\max}$.
2) $A_1(x) + \alpha_1 A_2(x) \leq 0$.

This LMI problem for finding the unknown constant parameters $c_{1,1}, \ldots, c_{1,N_1}$ and $c_{2,1}, \ldots, c_{2,N_2}$ is solved using YALMIP toolbox [21] for MATLAB ®.

C. Convergence Rate Control

Considering the results of Theorem 1, a control strategy can be defined to accelerate the convergence rate of the system. This is done with the following corollary.

Corollary 2: If the conditions of Theorem 1 are verified, the feedback control parameters $\tilde{u}$ can be calculated to obtain the following equality:

$$\int_0^1 x^2 p_1(x) \frac{\partial}{\partial x} \left(a_4(x) \tilde{j}_{\text{aux}}(\tilde{u}, x, t) \right) \tilde{z} dx$$
$$+ \gamma \int_0^1 \frac{x^2 p_2(x)}{\varepsilon} b_5(x) \tilde{Q}_{\text{aux}}(\tilde{u}, x, t) \tilde{T}_e dx = -\alpha_2 V \quad (13)$$

where $\alpha_2 > 0$ is a tuning parameter. Using this feedback control, the system (4) with boundary conditions (5) is globally exponentially stable and the convergence rate of the Lyapunov function satisfies $\dot{V} \leq -\beta_2 V$, where $\beta_2 = (\alpha_1 + \alpha_2)/[\max_{x \in [0,1]} (p_1(x), p_2(x))]$.

The convergence rate is thus increased by a factor $\alpha_2/[\max_{x \in [0,1]} (p_1(x), p_2(x))]$ by designing a control law that solves (implicitly) (13) for $\tilde{u}$.

Note that this controller is suitable for systems with commensurate time scales, such as small-scale tokamaks, but is not effective enough to improve the convergence rate of a system with different time scales [19]. The control strategy for large tokamaks is discussed in Section V.

V. System Decoupling Using Singular Perturbation Theory

In large tokamaks, the dynamics of z is much slower than the dynamics of T_e [25]. The system of PDEs (4)–(6) can thus be divided into two different time scales by introducing the fast time scale $\tau = \varepsilon t$. Singular perturbation theory is applied by isolating the slow variables, which are considered as fixed in the fast time scale and solved using static equations (thus separated from the fast component).

Considering that $\varepsilon \ll 1$, the electrons temperature dynamics can be decomposed into two components: the slow component $\tilde{T}_s$ that evolves with the (slow) variations of the magnetic flux and the fast component $\tilde{T}_f$ that reacts more rapidly to inputs variation. We thus have $\tilde{T}_e = \tilde{T}_s + \tilde{T}_f$. At the slow time scale, the static equation for the electron temperature is computed using the assumption that $\partial \tilde{T}_s / \partial \tau \ll \partial \tilde{T}_f / \partial \tau$ in the heat equation. In this equation, $\tilde{T}_e$ is replaced by $\tilde{T}_s$, which denotes the slow variation of the temperature. $\tilde{T}_s$ is called the quasi-steady state and is determined by

$$0 = \frac{1}{x} \frac{\partial}{\partial x} \left(x b_1(x) \frac{\partial \tilde{T}_s}{\partial x} \right) - b_2(x) \tilde{T}_s + \frac{1}{x} \frac{\partial}{\partial x} (x b_3(x) \tilde{z})$$
$$+ \frac{b_4(x)}{x} \left(\frac{\partial}{\partial x} (x \tilde{z}) \right) + b_5(x) \tilde{Q}_{\text{aux},s}(\tilde{u}_s, x, t) \quad (14)$$

where $\tilde{u}_s$ is the slow component of the input and with boundary conditions $(\partial \tilde{T}_s / \partial x)(0, t) = 0$ and $\tilde{T}_s(1, t) = \tilde{T}_{e,\text{edge}}(t)$. The solution of $\tilde{T}_s(x, t)$ is calculated at each time instant from $\tilde{z}$ and $\tilde{u}_s$ in (14) using numerical methods. The evolution of the fast dynamics is included with a boundary layer model, obtained in the fast time scale as

$$\frac{\partial \tilde{T}_f}{\partial \tau} = \frac{1}{x} \frac{\partial}{\partial x} \left(x b_1(x) \frac{\partial \tilde{T}_f}{\partial x} \right) - b_2(x) \tilde{T}_f$$
$$+ b_5(x) \tilde{Q}_{\text{aux},f}(\tilde{u}_f, x, \tau) \quad (15)$$

with boundary conditions

$$\frac{\partial \tilde{T}_f}{\partial x}(0, \tau) = 0 \quad \tilde{T}_f(1, \tau) = 0 \quad (16)$$

where $\tilde{u}_f$ stands for the fast component of the input.

The magnetic field component $\tilde{z}$ writes in terms of $\tilde{T}_s$ as

$$\frac{\partial \tilde{z}}{\partial t} = \frac{\partial}{\partial x} \left(\frac{a_1(x)}{x} \frac{\partial}{\partial x} (x \tilde{z}) \right) + \frac{\partial}{\partial x} (a_2(x) \tilde{T}_s)$$
$$+ \frac{\partial}{\partial x} \left(a_3(x) \frac{\partial \tilde{T}_s}{\partial x} \right) + \frac{\partial}{\partial x} (a_4(x) \tilde{z})$$
$$+ \frac{\partial}{\partial x} \left(a_5(x) \tilde{j}_{\text{aux}}(u_s, x, t) \right) \quad (17)$$

with boundary conditions

$$\tilde{z}(0, t) = 0 \quad \tilde{z}(1, t) = 0. \quad (18)$$

Our dynamics is thus composed of two PDEs at evolving at different time scales, (15) and (17) with their boundary and initial conditions, and one PDE that acts as an algebraic constraint (14) with its boundary conditions. The composite control is obtained by separately calculating and combining the slow and the fast components as $\tilde{u} = \tilde{u}_s + \tilde{u}_f$.

This article has been accepted for inclusion in a future issue of this journal. Content is final as presented, with the exception of pagination.

MAVKOV *et al.*: DISTRIBUTED CONTROL OF COUPLED INHOMOGENEOUS DIFFUSION IN TOKAMAK PLASMAS

5

A. Slow Component Stability and Control

The slow component of the control is calculated by considering only the magnetic flux dynamics (17) and the following Lyapunov function candidate is chosen:

$$V_s(\tilde{z}) = \frac{1}{2} \int_0^1 x^2 p_s(x) \tilde{z}^2 dx. \tag{19}$$

The evolution of this Lyapunov function is inferred from the following theorem.

Theorem 2: Suppose that for a given positive number α_3, there exists a polynomial p_s, such that $p_s(x) > 0$ for all $x \in [0, 1]$ and satisfying, for all $x \in [0, 1]$

$$\frac{a_1(x)}{2} \left(3xp_s'(x) + x^2 p_s''(x) - p_s(x) \right)$$
$$+ \frac{a_1'(x)}{2} \left(x^2 p_s'(x) + 3xp_s(x) \right) + \frac{x^2}{2} a_4'(x) p_1(x)$$
$$+ a_4(x) \left(xp_s(x) + \frac{x^2}{2} p_1'(x) \right) \leq -\frac{\alpha_3}{2} x^2. \tag{20}$$

Then, the time derivative $\dot{V}_s$ of the function V_s defined by (19) verifies

$$\dot{V}_s \leq -\beta_3 V_s + \int_0^1 x^2 p_s(x) \frac{\partial}{\partial x} \left(a_2(x) \tilde{T}_s + a_3(x) \frac{\partial \tilde{T}_s}{\partial x} \right) \tilde{z} dx$$
$$+ \int_0^1 x^2 p_s(x) \frac{\partial}{\partial x} \left(a_5(x) \tilde{j}_{\text{aux}}(\tilde{u}_s, x, t) \right) \tilde{z} dx \tag{21}$$

where $\beta_3 = (\alpha_3 / \max_{x \in [0,1]} p_s(x))$

Proof: See [24]. □

We use the dynamics (21) to design a convergence rate controller, as described in the following corollary.

Corollary 3: If the conditions of Theorem 2 are verified, the feedback control parameters of the slow component $\tilde{u}_s$ can be calculated to obtain the following relation:

$$\int_0^1 x^2 p_s(x) \frac{\partial}{\partial x} \left(a_2(x) \tilde{T}_s + a_3(x) \frac{\partial \tilde{T}_s}{\partial x} \right) \tilde{z} dx$$
$$+ \int_0^1 x^2 p_s(x) \frac{\partial}{\partial x} \left(a_5(x) \tilde{j}_{\text{aux}}(\tilde{u}_s, x, t) \right) \tilde{z} dx = -\alpha_4 V_s \tag{22}$$

where $\alpha_4 > 0$ is a tuning parameter. Using this feedback control, the system (17) with boundary conditions (18) is globally exponentially stable with a convergence rate that satisfies $\dot{V}_s \leq -\beta_4 V_s$, where $\beta_4 = ((\alpha_3 + \alpha_4) / \max_{x \in [0,1]} p_s(x))$.

B. Fast Component Stability and Control

The fast component of the system has dynamics governed by (15) and (16). To compute the stability of this system (boundary layer system), the following candidate Lyapunov function is selected:

$$V_f(\tilde{T}_f) = \frac{1}{2} \int_0^1 p_f(x) \tilde{T}_f^2 dx \tag{23}$$

and its dynamics is studied in the following theorem.

Theorem 3: Suppose that for a given positive number α_5, there exists a polynomial p_f, such that $p_f(x) > 0$ for all $x \in [0, 1]$ and satisfying, for all $x \in [0, 1]$

$$\frac{b_1(x)}{2} \left(x^2 p_f''(x) + 2xp_f'(x) + p_f(x) \right)$$
$$+ \frac{b_1'(x)}{2} \left(x^2 p_f'(x) + xp_f(x) \right) - x^2 b_2(x) p_f(x) \leq -\frac{\alpha_5}{2} x^2. \tag{24}$$

Then, the time derivative $\dot{V}_f$ of the function V_f defined by (23) verifies

$$\dot{V}_f \leq -\beta_5 V_f + \int_0^1 x^2 p_f(x) b_5(x) \tilde{Q}_{\text{aux},f}(\tilde{u}_f, x, \tau) \tilde{T}_f dx \tag{25}$$

where $\beta_5 = (\alpha_5 / \max_{x \in [0,1]} p_f(x))$.

Proof: See [24]. □

The convergence rate of the boundary layer system is controlled using the following corollary.

Corollary 4: If the conditions of Theorem 3 are verified, the feedback control parameters of the boundary layer system $\tilde{u}_f$ can be calculated to obtain the following relation:

$$\int_0^1 x^2 p_f(x) b_5(x) \tilde{Q}_{\text{aux},f}(\tilde{u}_f, x, \tau) \tilde{T}_f dx = -\alpha_6 V_f \tag{26}$$

where $\alpha_6 > 0$ is a tuning parameter. Using this feedback control, the system (15) with boundary conditions (16) is globally exponentially stable with a convergence rate that satisfies $\dot{V} \leq -\beta_6 V$, where $\beta_6 = ((\alpha_5 + \alpha_6) / \max_{x \in [0,1]} p_f(x))$.

Numerical algorithms to solve the functional equation (20) to find p_s from Theorem 2 and the functional equation (24) for p_f from Theorem 3 can be found in [4] and [5]. In this article, these inequalities are scalar and they are found using Legendre polynomials and the algorithm solving the LMI problem, as the one defined in Section IV-B.

VI. CONTROL IMPLEMENTATION

A. Auxiliary Current and Power Density Models

The auxiliary sources are modeled as simple weighted Gaussian distributions as proposed in [31], with the analytical parameterization defined for RAPTOR in [10]. These distributions approximate both the power and current densities. The total auxiliary current density is computed as the sum of the current densities induced by each EC antenna

$$j_{\text{aux}} = \sum_{i=1}^{n_{\text{aux}}} \frac{\overline{T}_e}{n_e} j_{\text{dis},i}(x) P_{\text{aux},i}(t) \tag{27}$$

where n_{aux} denotes the number of the auxiliary sources and $j_{\text{dis},i}(x)$ is a weighted Gaussian distribution (given in [10]), representing the normalized reference current density profile generated by the input powers $P_{\text{aux},i}(t)$ and the current-drive efficiency $(\overline{T}_e / n_e)$.

Similarly, the total auxiliary power density is composed by the sum of the individuals induced by each EC antenna

$$Q_{\text{aux}} = \sum_{i=1}^{n_{\text{aux}}} Q_{dis,i}(x) P_{\text{aux},i}(t) \tag{28}$$

where $Q_{\text{dis},i}(x)$ (given in [10]) is a normalized reference power density deposition profile for the ith auxiliary source. In our control application, $Q_{\text{dis},i}(x)$ and $j_{dis,i}(x)$ are fixed by the choice of the position and distribution of the EC antennas. Only the input powers $P_{\text{aux},i}(t)$ are thus available to achieve the desired control signals and $u(t) = [P_{\text{aux},1}(t), \ldots, P_{\text{aux},n_{\text{aux}}}(t)]$.

B. Calculation of the Control Inputs

The control is implemented using only a limited number of actuators (the powers of the EC clusters $P_{\text{aux},i}(t)$), while our convergence rate controllers imply the evolution of full spatial distributions. An extra step is thus needed to optimize the engineering parameters according to the control objective. This is achieved by solving (e.g., for Corollary 2) the following optimization problem at each time instant:

$$\min_{\tilde{u}} \quad J(\tilde{u})$$
$$\text{s.t.} \ -\alpha_2 V \leq J(\tilde{u}) \leq 0$$
$$\tilde{u}_{\min} \leq \tilde{u} \leq \tilde{u}_{\max} \qquad (29)$$

with

$$J(\tilde{u}) = \int_0^1 x^2 \, p_1(x) \frac{\partial}{\partial x}\big(a_4(x)\tilde{j}_{\text{aux}}(\tilde{u}, x)\big)\tilde{z}\,dx$$
$$+ \int_0^1 x^2 \frac{\gamma \, p_2(x)}{\varepsilon} b_5(x)\tilde{Q}_{\text{aux}}(\tilde{u}, x)\tilde{T}_e\,dx$$

where $\tilde{u}_{\min}$ and $\tilde{u}_{\max}$ stand for the minimum and maximum values of the allowed power for each antenna.

Remark 1: The convergence rate of the system in this section is calculated from a practical implementation standpoint. It takes into account the limitations of the current and of the power distribution profiles, imposed by the limitations of the auxiliary heating sources. These limitations make the equality (13) to be very restrictive and difficult to achieve. The optimization (29) solves the optimal engineering parameters to reach the desired convergence rate α_2 in a less strict way. Therefore, the closed-loop system is stable and the convergence rate varies in the range: $-\beta_1 \, V \leq \dot{V} \leq -\beta_2 \, V$ (between the open-loop and unconstrained control values), depending on the actuators limitations.

The decoupling control implies two objective functions: one for the slow (22) and one for the fast component (26). Combining these two functions for feedback control design, the following multiobjective optimization problem is formulated:

$$\min_{\tilde{u}=\tilde{u}_s+\tilde{u}_f} \quad \omega_1 \, J_s(\tilde{u}_s) + \omega_2 \, J_f(\tilde{u}_f)$$
$$\text{s.t.} \ -\alpha_4 \mathcal{V}_s \leq J_s(\tilde{u}_s) \leq 0$$
$$-\alpha_6 \mathcal{V}_f \leq J_f(\tilde{u}_f) \leq 0$$
$$\tilde{u}_{\min} \leq \tilde{u}_s + \tilde{u}_f \leq \tilde{u}_{\max} \qquad (30)$$

with

$$J_s(\tilde{u}_s) = \int_0^1 x^2 \, p_s(x) \frac{\partial}{\partial x}\left(a_2(x)\tilde{T}_s + a_3(x)\frac{\partial \tilde{T}_s}{\partial x}\right)\tilde{z}\,dx$$
$$+ \int_0^1 x^2 \, p_s(x) \frac{\partial}{\partial x}\big(a_5(x)\tilde{j}_{\text{aux}}(\tilde{u}_s, x)\big)\tilde{z}\,dx$$

$$J_f(\tilde{u}_f) = \int_0^1 x^2 \, p_f(x)b_5(x)\tilde{Q}_{\text{aux},f}(\tilde{u}_f, x)\tilde{T}_f\,dx.$$

The weights ω_1, $\omega_2 > 0$ are tuning parameters and $\tilde{T}_s$ is found as the solution of (14) at each time instant using $\tilde{z}$ and $\tilde{u}_s$.

VII. RESULTS

The two control strategies are evaluated using the nonlinear tokamak simulator RAPTOR. While real tokamak experiments for feedback control purposes are particularly difficult to obtain, RAPTOR provides a valid alternative as it includes the main physical properties of the plasma at the time scales of this article and has been successfully compared with experimental measurements on numerous test cases. Furthermore, RAPTOR can be runned outside of the control environment as a simulator in stand-alone situation as well as being used as an estimator for the control algorithms implemented in the actual tokamak control system, when implemented. Using RAPTOR as a reference simulator is thus particularly relevant for control design evaluation [1], [9], [10], [14], [22], [29]. We chose to focus the simulation results on the impact of the different time scales only, due to space limitations. Analysis and simulation results related to robustness and to the impact of extra additional heatings can be found in [6], [7], and [23].

Our control approaches are evaluated and compared on the tokamak configuration of ITER ($\epsilon \approx 0.01$) in L-mode, emphasizing the interest for considering the different time scales separately for large tokamaks. Three EC antennas are used as actuators. The plasma current is set to a constant $I_p = 7\,\text{MA}$ and a linearized model is obtained by extracting the parameters corresponding to a stationary state when constant values of the powers of the EC antennas are $P_{\text{ec1}} = P_{\text{ec2}} = P_{\text{ec3}} = 7$ MW. The input powers are limited in the range of 0–10 MW. Several reference profiles are obtained to test the controllers performance. An additional EC antenna is introduced to test the robustness with respect to deviations from the calculated equilibrium point.

Since both control methods ask for a choice concerning the relative importance of the magnetic flux control with respect to the electrons heat control, we consider two control cases: Case 1 emphasizes the convergence rate of $\tilde{z}$, while $\tilde{T}_e$ is the priority for Case 2. Both control methods are evaluated on each case.

We first implement the coupled control presented in Section IV. The convergence rate is set by the tuning parameter α_1 and the nature of the response depends highly on the choice of the scaling parameter γ [which multiplies $\tilde{T}_e$ in the Lyapunov function (7)]. When γ is low (Case 1), the control is more effective for the performance of the slow variable $\tilde{z}$, while the convergence rate of T_e is difficult to tune (typically enduring high overshoots). When the value of γ is high (Case 2), the performance of the convergence rate of T_e can be tuned, but the convergence rate of $\tilde{z}$ is free. To improve the convergence rate of $\tilde{z}$, we need in this case to increase the value of α_1, which induces oscillations in the T_e profile. The results from these simulations are presented in Fig. 1. While the convergence of ι and T_e is achieved in both control cases, the disparity in the convergence rates of the
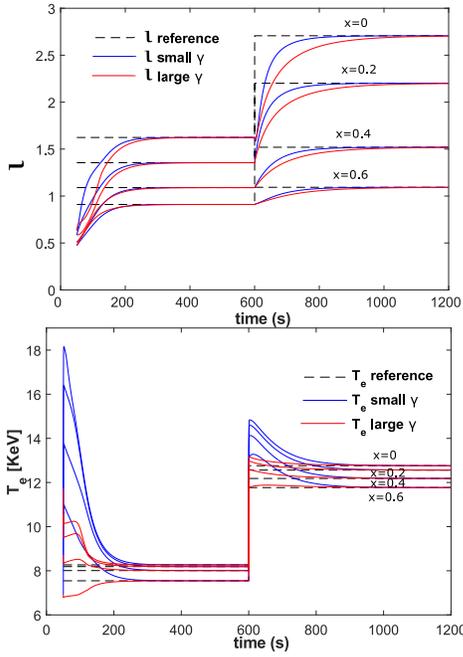
Fig. 1. Evolution ι (top) and T_e (bottom) in the ITER simulation with the coupled controller and with convergence priority given to $\tilde{z}$ (Case 1, small γ) or $\tilde{T}_e$ (Case 2, large γ).
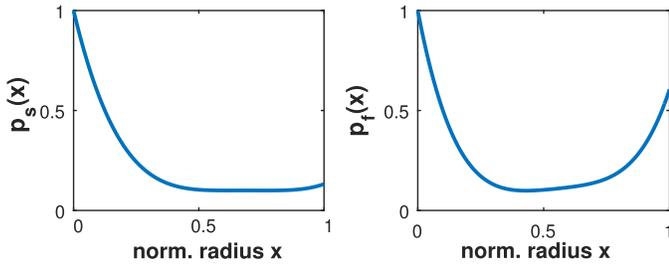

Fig. 2. Numerical solution of the composite control polynomials p_s and p_f for ITER.

Fig. 3. Evolution of T_e and ι in the ITER simulation with composite control for Cases 1 and 2.

Fig. 4. Time evolution of the two normalized Lyapunov functions of the composite control (V_s and V_f) for the ITER simulation.

two dynamics renders the relative tuning particularly difficult to achieve, motivating the system decoupling approach.

We now apply the composite control presented in Section V. The polynomials of the Lyapunov functions, presented in Fig. 2, are computed separately for the fast and the slow components. The maximum values of the convergence rate parameters are calculated numerically as $\alpha_4 = 0.01$ and $\alpha_7 = 9.3$. The difference between these two values was expected due to the difference in the time scales. The solution of the slow component of the temperature (14) is numerically calculated at each time instant and subtracted from $\tilde{T}_e$ to estimate the fast component of the temperature $\tilde{T}_f$. The output parameters $\iota(x, t)$ and $T_e(x, t)$ at several locations are presented in Fig. 3 for the two control cases. For Case 1, a feedback control is applied only on the slow component of the system. The results from this simulation have a similar performance as in the case when the method presented in Section IV is applied and low γ is used. For Case 2, the composite control combines the feedback control of the fast and slow components. The effect of the feedback
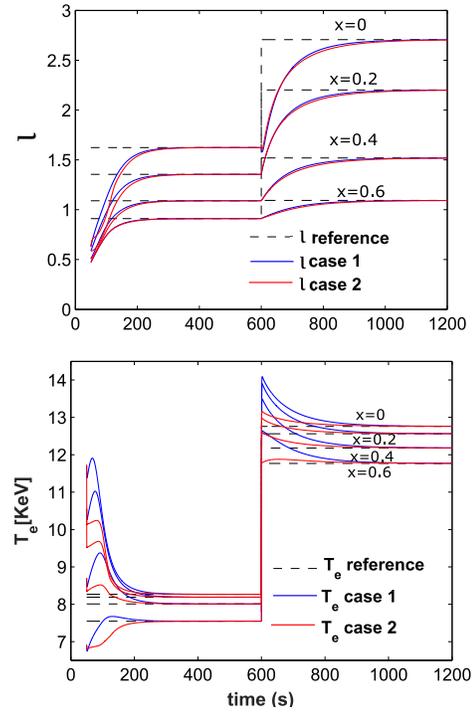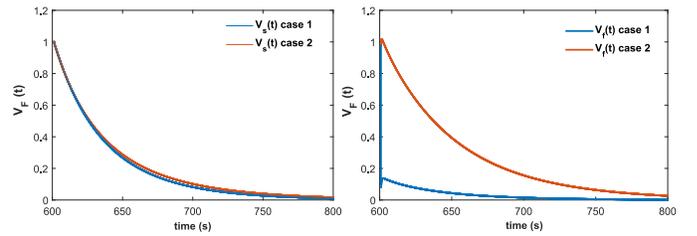
control on the boundary layer system can be observed on $T_e(x, t)$: applying a control on the boundary layer system results in a reduced overshoot and a better convergence of the fast component at the cost of a slower convergence of the slow component. This behavior is also observed on the time evolution of the Lyapunov function in Cases 1 and 2 starting from $t = 600$ s (when the reference profiles are changed) in Fig. 4.

The tuning of the closed-loop performance with the composite control can be done by changing the values of the weighting parameters $\omega_{1,2}$ to obtain the desired balance between the two components. The convergence rate of the closed-loop system is selected by the choice of α_4 and α_6 for the performance of the slow and fast component, respectively. Increasing the value of α_4 decreases the settling time and decreases the steady-state error of the slow component, but increases the overshoot of the electron temperature. By increasing the value of α_6, the convergence rate of the fast component is improved and the overshot of the electron temperature is decreased. If α_6 is increased further, it leads to high oscillations of the fast

This article has been accepted for inclusion in a future issue of this journal. Content is final as presented, with the exception of pagination.

8   IEEE TRANSACTIONS ON CONTROL SYSTEMS TECHNOLOGY

varying component. Note also that when the two control functions are calculated separately, we can apply different sampling periods for the two parameters, which improves the computational efficiency and the performance of the feedback control.

VIII. CONCLUSION AND FUTURE WORK

Integrated feedback control algorithms for coupled current and electron temperature profiles in tokamaks are developed and tested in this article. The plasma states are modeled as two coupled inhomogeneous 1-D diffusion PDEs, and a control-oriented model is proposed using linearized simple models for the controlled plasma parameters. The control design is based on the infinite-dimensional settings by using the control Lyapunov functions. Our first control method is based on the coupled dynamics and on a single Lyapunov function. The different time scales of the two states motivated a second control strategy designed by decoupling the two time scales of the system using the singular perturbation theory. Both controllers are evaluated using the nonlinear RAPTOR tokamak plasma simulator, parameterized for ITER. The different times scales permit us to compare the two control strategies. In the future, our control strategies can be used in a real tokamak machine using the state observer for the plasma profiles developed in [8]. A future perspective is also to consider the ohmic heating sources in the control design, as a boundary input.

ACKNOWLEDGMENT

REFERENCES

[1] J. E. Barton, W. P. Wehner, E. Schuster, F. Felici, and O. Sauter, "Simultaneous closed-loop control of the current profile and the electron temperature profile in the TCV tokamak," in *Proc. Amer. Control Conf.*, Chicago, IL, USA, 2015, pp. 3316–3321.

[2] M. D. Boyer *et al.*, "First-principles-driven model-based current profile control for the DIII-D tokamak via LQI optimal control," *Plasma Phys. Control. Fusion*, vol. 55, no. 10, p. 105007, 2013.

[3] M. D. Boyer *et al.*, "Backstepping control of the toroidal plasma current profile in the DIII-D tokamak," *IEEE Trans. Control Syst. Technol.*, vol. 22, no. 5, pp. 1725–1739, Sep. 2014.

[4] F. Bribiesca Argomedo, C. Prieur, E. Witrant, and S. Brémond, "A strict control Lyapunov function for a diffusion equation with time-varying distributed coefficients," *IEEE Trans. Autom. Control*, vol. 58, no. 2, pp. 290–303, Feb. 2013.

[5] F. Bribiesca Argomedo, E. Witrant, and C. Prieur, "D^1-input-to-state stability of a time-varying nonhomogeneous diffusive equation subject to boundary disturbances," in *Proc. Amer. Control Conf.*, Montreal, QC, Canada, 2012, pp. 2978–2983.

[6] F. Bribiesca Argomedo, E. Witrant, and C. Prieur, *Safety Factor Profile Control in a Tokamak*. New York, NY, USA: Springer, 2014.

[7] F. B. Argomedo, E. Witrant, C. Prieur, S. Brémond, R. Nouailletas, and J.-F. Artaud, "Lyapunov-based distributed control of the safety-factor profile in a tokamak plasma," *Nucl. Fusion*, vol. 53, no. 3, p. 033005, 2013.

[8] F. Felici, M. de Baar, and M. Steinbuch, "A dynamic state observer for real-time reconstruction of the tokamak plasma profile state and disturbances," in *Proc. Amer. Control Conf.*, Portland, OR, USA, 2014, pp. 4816–4823.

[9] F. Felici and O. Sauter, "Non-linear model-based optimization of actuator trajectories for tokamak plasma profile control," *Plasma Phys. Control. Fusion*, vol. 54, no. 2, p. 025002, 2012.

[10] F. Felici *et al.*, "Real-time physics-model-based simulation of the current density profile in tokamak plasmas," *Nucl. Fusion*, vol. 51, no. 8, p. 083052, 2011.

[11] A. Gahlawat, E. Witrant, M. M. Peet, and M. Alamir, "Bootstrap current optimization in tokamaks using sum-of-squares polynomials," in *Proc. 51st Annu. Conf. Decision Control*, 2012, pp. 4359–4365.

[12] Z. Gajic, *Optimal Control of Singularly Perturbed Linear Systems and Applications*. Boca Raton, FL, USA: CRC Press, 2001.

[13] O. Gaye, L. Autrique, Y. Orlov, E. Moulay, S. Brémond, and R. Nouailletas, "H_∞ stabilization of the current profile in toka-mak plasmas via an LMI approach," *Automatica*, vol. 49, no. 9, pp. 2795–2804, 2013.

[14] P. Geelen, F. Felici, A. Merle, and O. Sauter, "Parameter estimation for a nonlinear control-oriented tokamak profile evolution model," *Plasma Phys. Control. Fusion*, vol. 57, no. 12, p. 125008, 2015.

[15] F. L. Hinton and R. D. Hazeltine, "Theory of plasma transport in toroidal confinement systems," *Rev. Mod. Phys.*, vol. 48, no. 2, p. 239, 1976.

[16] W. Kaplan, *Advanced Calculus*. Reading, MA, USA: Addison Wesley, 2002.

[17] H. K. Khalil, *Nonlinear Systems*, 3rd ed. Upper Saddle River, NJ, USA: Prentice-Hall, 2002.

[18] S. H. Kim and J. Lister, "A potentially robust plasma profile control approach for ITER using real-time estimation of linearized profile response models," *Nucl. Fusion*, vol. 52, no. 7, p. 074002, 2012.

[19] P. Kokotovic, H. K. Khalil, and J. O'Reilly, *Singular Perturbation Methods in Control: Analysis and Design*, vol. 25. Philadelphia, PA, USA: SIAM, 1999.

[20] L. Laborde *et al.*, "A model-based technique for integrated real-time profile control in the JET tokamak," *Plasma Phys. Control. Fusion*, vol. 47, no. 1, p. 155, 2005.

[21] J. Löfberg, "YALMIP: A toolbox for modeling and optimization in MATLAB," in *Proc. IEEE Int. Symp. Comput. Aided Control Syst. Design*, Taipei, Taiwan, Sep. 2004, pp. 284–289.

[22] E. Maljaars *et al.*, "Profile control simulations and experiments on TCV: A controller test environment and results using a model-based predictive controller," *Nucl. Fusion*, vol. 57, no. 12, p. 126063, 2017.

[23] B. Mavkov, "Control of coupled transport in tokamak plasmas," Ph.D. dissertation, Grenoble Alps Univ., Grenoble, France, 2017.

[24] B. Mavkov, E. Witrant, and C. Prieur, "Distributed control of coupled inhomogeneous diffusion in tokamak plasmas (full version)," HAL, Tech. Rep. hal-01545010, 2017. [Online]. Available: http://hal.archives-ouvertes.fr/hal-01545010/

[25] D. Moreau *et al.*, "A two-time-scale dynamic-model approach for magnetic and kinetic profile control in advanced tokamak scenarios on JET," *Nucl. Fusion*, vol. 48, no. 10, p. 106001, 2008.

[26] A. Pironti and M. Walker, "Fusion, tokamaks, and plasma control: An introduction and tutorial," *IEEE Control Syst.*, vol. 25, no. 5, pp. 30–43, Oct. 2005.

[27] Y. Tang, C. Prieur, and A. Girard, "Tikhonov theorem for linear hyperbolic systems," *Automatica*, vol. 57, pp. 1–10, Jul. 2015.

[28] R. Vazquez and M. Krstic, *Control of Turbulent and Magnetohydro-dynamic Channel Flows: Boundary Stabilization and State Estimation*. Basel, Switzerland: Birkhäuser, 2008.

[29] N. M. T. Vu, R. Nouailletas, L. Lefèvre, and F. Felici, "Plasma q-profile control in tokamaks using a damping assignment passivity-based approach," *Control Eng. Pract.*, vol. 54, pp. 34–45, Sep. 2016.

[30] J. Wesson, *Tokamaks* (International Series of Monographs on Physics), vol. 149, 4th ed. Oxford, U.K.: Oxford Univ. Press, 2011.

[31] E. Witrant *et al.*, "A control-oriented model of the current profile in tokamak plasma," *Plasma Phys. Control. Fusion*, vol. 49, no. 7, p. 1075, 2007.